Nano Research

ISSN 1998-0124 CN 11-5974/O4
https://doi.org/10.1007/s12274-024-6516-6

Research Article

High precision patternable liquid metal based conductor and adhesive substrate enabled stretchable hybrid systems

Runhui Zhou[1,2,§], Jiaoya Huang[1,§], Zemin Li[1,2], Yushu Wang[3], Ziyu Chen[3], and Caofeng Pan[1,2,4] (✉)

[1] *CAS Center for Excellence in Nanoscience, Beijing Key Laboratory of Micro-nano Energy and Sensor, Beijing Institute of Nanoenergy and Nanosystems, Chinese Academy of Sciences, Beijing 101400, China*
[2] *School of Nanoscience and Engineering, University of Chinese Academy of Sciences, Beijing 100049, China*
[3] *Center on Nanoenergy Research, School of Physical Science and Technology, Guangxi University, Nanning 530004, China*
[4] *Institute of Atomic Manufacturing, Beihang University, Beijing 100191, China*
[§] *Runhui Zhou and Jiaoya Huang contributed equally to this work.*

Received: 23 December 2023 / **Revised:** 24 January 2024 / **Accepted:** 25 January 2024

ABSTRACT

Stretchable hybrid systems have been attracting tremendous attention for their essential role in soft robotics, on-skin electronics, and implantable devices. Both rigid and soft functional modules are typically required in those devices. Consequently, ensuring stable electrical contact between rigid and soft modules is a vital part. Here, we propose a simple, universal, and scalable strategy for the stretchable hybrid system through a highly precise printable liquid metal particle-based conductor and adhesive fluorine rubber substrate. The properties of liquid metal particle-based conductors could be easily tuned to realize high-precision patterning, large-scale printing, and the ability to print on various substrates. Additionally, the fluorine rubber substrate could form strong interfacial adhesion with various components and materials through simply pressing and heating, hence enabling stable electrical contact. Furthermore, we prepared a stretchable hybrid light-emitting diode (LED) display system and employed it in on-skin visualization of pressure levels, which perfectly combined rigid and soft modules, thus demonstrating the promising potential applications in complex multifunctional stretchable hybrid systems for emerging technologies.

KEYWORDS

stretchable hybrid systems, liquid metal, high precision, interfacial adhesion

1 Introduction

With the development of technology, stretchable systems possess enormous prospects in various fields including soft robotics [1–4], skin electronics [5–8], wearable devices [9–12], and implantable devices [13–15]. In order to meet the diverse functional requirements, it is necessary to integrate rigid modules like Si-based microelectronics to form hybrid devices [16–18]. In general, stretchable hybrid devices can be divided into three elementary components, stretchable conductors that connect each functional part, substrates that possess desired mechanical properties, and functional parts comprising rigid microelectronic devices. Hence, stretchable conductors that can be simply patterned with high resolution on a large scale are essential for multifunctional stretchable electronic systems. In addition, due to the mechanical mismatches between the rigid modules of microelectronic devices and the soft modules of stretchable conductors and substrates, the contact points of the stretchable systems could easily suffer from interfacial failure under deformation [19, 20]. Therefore, the key point is to realize the simple, precise, universal, and large-scale manufacturing of patterned stretchable conductors and the interface stability between the rigid and soft modules.

Various approaches have been attempted, and in terms of stretchable conductors, the main design strategies focused on three aspects. First, plenty of structure designs that convert in-plane strain into out-of-plane strain to maintain conductivity under deformation have been reported, including serpentine [18, 21, 22], mesh [12, 23, 24], microcracks [25, 26], and Longitudinal wave structures [27–29]. Second, intrinsically stretchable conductors that could simultaneously possess stretchability and conductivity have been extensively studied, such as conductive polymers [30–32], ionic conductors [33–35], and liquid metals [36–38]. Third, another approach is to disperse conductive fillers (for instance, metal nanomaterials [39–42], carbon nanotube (CNT) [43], Mxene [44–47], graphene [48], and conductive polymers [49]) into a polymer matrix forming uniform conductive composites. The conductivity of the stretchable composites relies on the percolation network of the conductive fillers; consequently, the applied strain would be diluted into the distance change between the enormous amount of conductive fillers to ensure the conductivity under deformation. Furthermore, the properties of the composites could be easily modulated by changing the types and contents of the components. Consequently, the composites could be regulated to obtain appropriate rheological and electrical properties that can meet the requirements of large-scale and high-precision printing methods. Therefore, this strategy is a promising approach to prepare the stretchable conductors for the stretchable systems.

However, in terms of enhancing the interface stability, there are

Address correspondence to pancaofeng@buaa.edu.cn

still many challenges in simply and rapidly enhancing the interface interactions among the multiple types of rigid and soft modules. Currently, the methods of enhancing the interface adhesion can be categorized into two strategies: through chemical or physical interactions. Firstly, chemical interactions were introduced to enhance interfacial adhesion, including covalent bonds [50–52] and supramolecular interactions [53–55]. However, pretreatment was normally needed to form chemical interactions; besides, not all materials were suitable to emanate chemical interactions. On the other hand, physical interactions such as molecular or mechanical interlock structures [56–58] and van der Waals interactions could form among various materials, but precise micro-nano fabrication was generally needed to construct specific structures to enhance the interfacial toughness.

Herein, we introduced a stretchable hybrid system design strategy by using an adhesive polymer as substrate and a high-precision patternable liquid metal (LM) particle-based conductor. The LM as a kind of low-melting point metal possesses high electrical conductivity of 3.4×10^4 S/cm and excellent fluidity under room temperature [36], which makes it extremely appropriate for stretchable conductors. Additionally, The LM could be dispersed into the fluorine rubber (FR) by probe ultrasonication. The rheological properties of the composite of LM and FR could be simply tuned by the content of the solvent. Hence, a high precision line width of 100 μm was achieved by the precise dispensing printing method. Meanwhile, the fluorine rubber which can form tough adhesion with electronic components by simply pressing and heating was used as the substrate to ensure the stable connectivity between the stretchable conductor and rigid electronic components. Therefore, a stretchable light-emitting diode (LED) display array was successfully prepared through the above-mentioned strategies. The LED array was further integrated with sensor signal acquisition and microcontroller into a hybrid system, which reveals the enormous potential in the application of integrated, wearable, and stretchable electronics.

2 Experimental

2.1 Materials

Liquid metal (EGaIn, Ga 75.5% and In 24.5% by weight) was purchased from Dongguan Huatai Metal Materials Technology Co., Ltd., fluorine rubber (DAI-EL G802) was purchased from Daikin Industries, and Ag nanoflakes (Ag flakes, 10 μm, > 99.9% trace metals basis) were purchased from Sigma Aldrich. 2-(2-Butoxyethoxy) ethyl acetate, 4-methyl-2-pentanone, poly(ethylene glycol) diacrylate (PEGDA) (average M_W = 1000), the photoinitiator Irgacure 184, and poly(vinyl alcohol) (PVA) (M_W = 31,000) were all purchased from Aladdin. All chemicals were used as received without further purification.

2.2 Preparation and patterning of LM composite

The liquid metal was first broken into microdroplets in 2-(2-butoxyethoxy) ethyl acetate by probe ultrasonication (VC 505, Sonics & Materials, INC.). Meanwhile, the fluorine rubber was dissolved in 4-methyl-2-pentanone at a concentration of 50% by weight. Then dissolved fluorine rubber was added to the LM dispersion and stirred with a magnetic stirrer for 30 min. The rheological properties of the LM composites could be easily adjusted by changing the content of the solvent to satisfy the requirements of different printing conditions. After the LM composite ink formation, the microelectronic printer (MP 1100A, Shanghai Mifang Electronic Technology Co., LTD.) was used to pattern the LM composite and the printing parameters could be adjusted to realize the high precision patterning.

2.3 Fabrication of the LM composite samples for electronic properties tests

First, 10% PVA water solution was spin-coated on the glass sheet (76.2 mm × 25.4 mm) which was washed with deionized water and ethyl alcohol, respectively. The fluorine rubber was resolved in 4-methyl-2-pentanone at a concentration of 25% by weight and PEGDA was added to enhance the mechanical performance. The mass ratio of fluorine rubber:PEGDA:Irgacure 184 was 100:6:3. Then the fluorine rubber solution was poured onto the glass sheet and placed on the hot plane to completely evaporate the solvent. Subsequently, the LM composite was stencil-printed onto the fluorine rubber substrates, and a composite of Ag nanoflakes and fluorine rubber was used to connect the LM composite and nickel conductive tape. After being encapsulated by fluorine rubber, the LM conductor samples were placed in water and kept in the oven at 60 °C for 10 h to release from the glass sheet. Subsequently, the LM conductor samples were put under ultraviolet light (365 nm, 50 W) for 20 min for the cross-linking of PEGDA.

2.4 Fabrication of the hybrid devices

First, the fluorine rubber was resolved in 4-methyl-2-pentanone at a concentration of 25% by weight. Next, the glass sheet was cleaned with deionized water and ethyl alcohol, respectively. After drying in an oven, 10% PVA water solution was spin-coated on the glass sheet and then dried in an oven at 80 °C for 30 min. Then the fluorine rubber solution was poured on the PVA coat glass sheet, and the glass sheet was placed in a fume hood to evaporate the solvent. The fluorine rubber substrate was prepared after the solvent completely evaporated. Subsequently, the LM composite was stencil-printed onto the fluorine rubber substrates, then the electronic components were placed at corresponding positions and heated to 80 °C to completely evaporate the solvent and form a strong adhesion. Then a composite of Ag nanoflakes and fluorine rubber was used to enhance the connection between LM composite and electronic components. After that, the fluorine rubber was used to encapsulate the device, and the device on the glass sheet was placed in water and kept in the oven at 60 °C for 10 h to release from the glass sheet.

2.5 Fabrication of stretchable hybrid system of pressure perception and display

The fluorine rubber substrate was first prepared on a 10 cm × 10 cm glass sheet by above mentioned method. Then the LM composite was patterned by stencil printing on the fluorine rubber substrate. Subsequently, the resistors and LEDs were placed at corresponding positions and the composite of Ag nanoflakes and fluorine rubber was used to enhance the electric contact. The integrated LED array was placed in an oven to completely evaporate the solvent. After that, the flexible printed circuit (FPC) cables were pressed on corresponding positions of the LED array, then it was placed in an oven at 80 °C for 2 h to form a strong adhesion. Next, the fluorine rubber was used to encapsulate the device. Subsequently, the stretchable hybrid system was released from the glass sheet after being placed in water and kept in the oven at 60 °C for 10 h.

2.6 Characterization

The morphologies of the printed LM lines and the LM particles were characterized using field-emission scanning electron microscopy (FE-SEM, SU1510 Hitachi). The adhesion test was performed using a tensile machine (YL-S70, Guangdong Yuelian Instruments Co., Ltd.). The electric responses of the samples under strain were tested on a customized high-precision electric displacement system (Beijing Feichuang Yida Optoelectronic

Technology Co., Ltd.), and the electrical responses were recorded by an electrochemical workstation (Autolab PGSTAT302N Metrohm). The pressure signals of the pressure sensor were measured by Multichannel data acquisition systems (National Instrumental, PXIe-4300).

3 Results and discussion

3.1 The design concept of the stretchable hybrid system

The main design concept of the stretchable hybrid system is schematically illustrated in Fig. 1. The LM was first broken into micro-particles through probe ultrasonication. The morphology of the LM particles is shown in Fig. S1 in the Electronic Supplementary Material (ESM). The size of the LM particles was uniform, with an average size of 4.3 μm, and the size distribution was concentrated at 2–7 μm. Then, the LM particles were blended with FR into a uniform composite by magnetic stirring. The composites could maintain good stability because of dipole–dipole interactions between the oxidation of LM and the C–F groups in FR [36]. Therefore, the rheological properties of the composites could be easily modulated to satisfy the requirements of high-precision printing methods. Furthermore, the electronic components could be stably adhered to the FR substrate by simply pressing and heating. Thus, the stretchable hybrid systems could be simply prepared by placing the electronic components at appropriate positions after the LM composites were printed.

3.2 Characterization of the high precision printing

The high-precision printing process of the LM-FR composite is shown in Fig. 2(a), and a large area of stretchable circuit was prepared. Additionally, the composite could also be precisely printed onto various substrates through the optimization of the printing parameters. As shown in Fig. 2(b), the precise patterning of the composite has been successfully achieved on various substrates including stretchable and unstretchable materials like polydimethylsiloxane (PDMS), FR, paper, and polyethylene terephthalate (PET), which revealed the universality and extensibility of this method. Additionally, the precise and large-scale printing on stretchable substrates was fundamental for the construction of stretchable hybrid systems because the patterned conductor basically determined the density, complexity, and stretchability of the system. Then, a stretchable circuit of 10 cm × 10 cm was printed on a thin PDMS substrate. The large area and flexibility of the printed circuit are demonstrated in Fig. 2(c). Furthermore, the printed circuit could remain intact under 50% strain, which demonstrated outstanding stretchability (Fig. 2(d) and Fig. S2 in the ESM). In addition, another key parameter of printed conductors was the line width which could affect the device density and the complexity of the system functions. Through the optimization of the content of solvent and the printing parameters, a high precision line width of 100 μm was realized (Fig. 2(e)), and uniform LM composite lines with varied line gaps were accurately prepared. The SEM image of the uniform lines with varied gaps is shown in Fig. 2(f). It was worth noting that the line gap was successfully reduced to 10 μm, and further reduction of the line gap could be possible with the utilization of more precise equipment. In addition, statistical analysis results of printed line width are shown in Figs. 2(g) and 2(h). The printed line width exhibited great consistency, with an average value of 100.317 μm, and the variation of the line width was highly concentrated within ±4%. The above results demonstrated the high precision, high spatial uniformity, and ability to be printed on various substrates of the patternable LM composites, which suggested the great potential in stretchable systems.

3.3 Characterization of the tough adhesion

Another key point of the realization of stretchable hybrid systems was the interfacial toughness. However, it was rather difficult to ensure stable interfacial adhesion among the varied rigid and soft modules. Previous works [5, 51, 59] generally only exhibited interfacial adhesion between specific materials or a small variety of modules in stretchable systems. Hence, a simple and universal method was needed. Here we proposed a simple, universal, and scalable method for interfacial adhesion in stretchable hybrid systems by using adhesive substrate. The fluorine rubber which can form strong adhesion with various electronic components by simply pressing and heating was used as substrate. As a proof of concept, we assembled an integrated electronics system of a stretchable LED array, as shown in Fig. 3(a). The LM composites were first stencil printed onto the FR substrate as conductors, and then the 37 LEDs with a package size of 0603 were placed on the corresponding positions. The LED array with the shape of "BINN" characters possessed uniform light emission, and it maintained nearly the same luminous intensity when stretched to 50% strain, which demonstrated the stable contact between the rigid modules of LEDs and the soft modules of LM electrodes and substrate under large strain. Then a memory chip was pressed on the FR substrates and heated to 80 °C, and the strong adhesion between the memory chip and the substrate is shown in Fig. 3(c). Further, we performed the adhesion test between the FR substrate and the

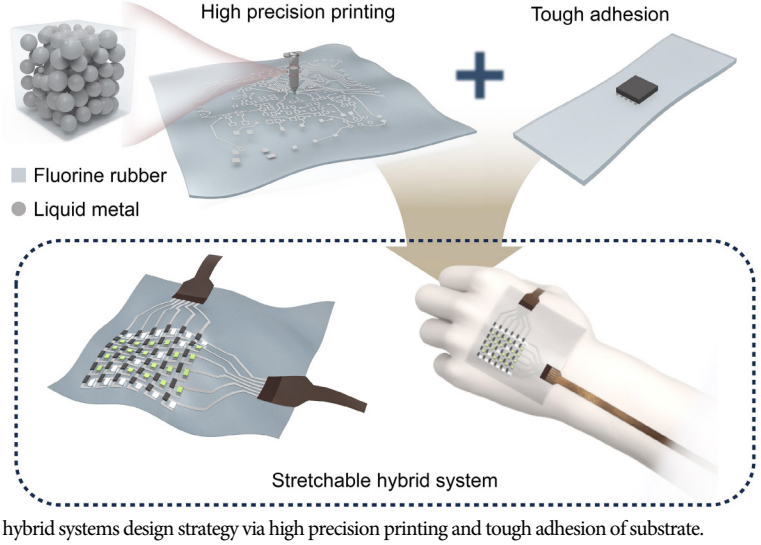

Figure 1 Illustration of stretchable hybrid systems design strategy via high precision printing and tough adhesion of substrate.

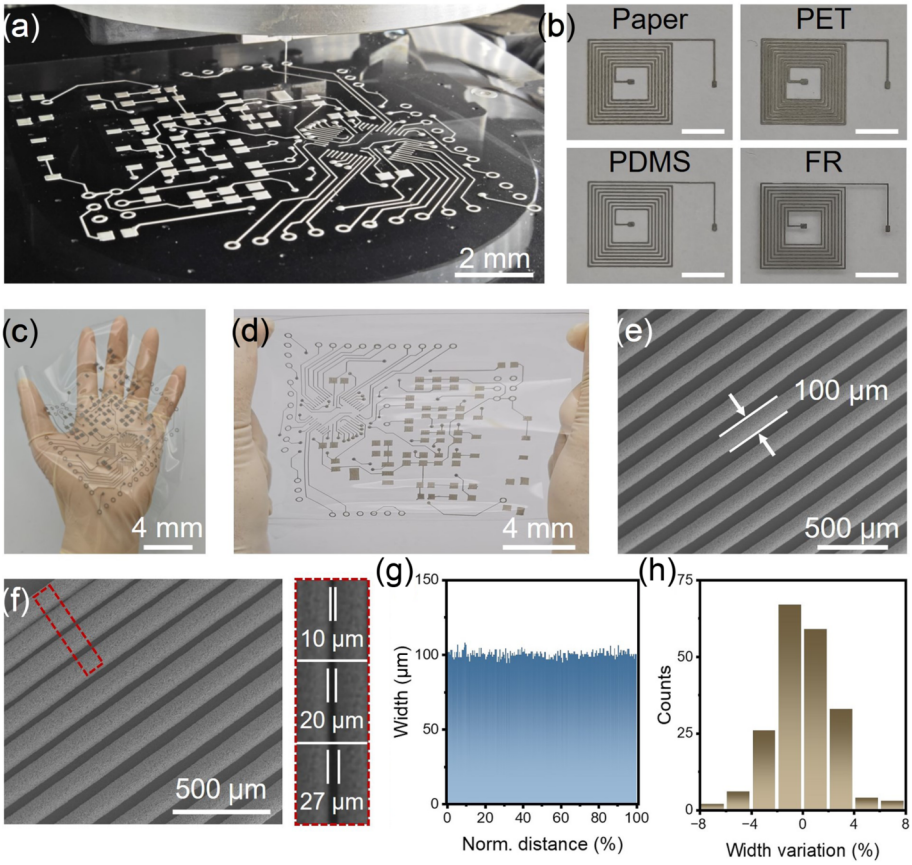

Figure 2 High-precision printing of the LM-FR composite conductors. (a) The optical image of the stretchable circuit fabricated by high-precision printing. (b) The high-precision printing of LM on various substrates. All the scale bar is 500 μm. (c) The optical image of the stretchable circuit printed on PDMS substrate. (d) The optical image of the circuit being stretched to 50% strain. (e) The SEM image of the printed LM lines with a line width of 100 μm. (f) The SEM image of the printed LM lines with varied gaps. (g) Corresponding line width distribution of the printed LM lines. (h) Corresponding line width variation of the printed LM lines.

various electronic components and common materials in the electronic circuit to illustrate the universality and extensibility of our strategy. Firstly, various electronic components including amplifier chips, chip inductors, chip capacitors, chip resistors, and crystal oscillators were simply pressed on the FR substrates by finger and then kept in the oven at 80 °C for 10 h to form tough interfacial adhesion. The results of the adhesion test are shown in Fig. 3(d). It can be observed that the FR substrate only possessed slightly lower adhesion strength with amplifier chips and chip inductors at 2.31 and 2.95 MPa, respectively, while the adhesion strength with other electronic components all exceeded 3.5 MPa, approaching 4 MPa. Furthermore, we performed the interfacial toughness tests between FR substrates and various common materials in electronic circuits including PET, glass, aluminum, steel, and copper. The results illustrated in Fig. 3(e) indicated that the FR substrates formed significant interfacial toughness with all the above-mentioned materials. Even the weakest interfacial toughness observed with glass surpassed 30 J/m^2. Remarkably, the interfacial toughness with metals was even higher, with the minimum interfacial toughness approaching 400 J/m^2 for copper and exceeding 450 J/m^2 for other metals. Moreover, to elucidate the stability of the stretchable hybrid system prepared by our proposed strategies under cyclic strain, we prepared three types of stretchable hybrid devices containing different components, including flexible flat cable, LED, and chip resistor. The corresponding electrical signals of different stretchable hybrid devices under the cyclic strain of 50% are exhibited in Figs. 3(f)–3(h), respectively. The corresponding electronic signals manifested a slight change under cyclic strain, which fully demonstrated the effectiveness of our proposed strategies. According to the results of the above tests, the rather strong interfacial adhesion with the multifarious rigid modules and simple treating process demonstrated great potential in compatibility with circuit manufacturing, processing capability of Si-based microelectronics, and novel fully stretchable system fabrication methods development.

3.4 The electrical properties of the LM composite conductor

Generally, the as-prepared LM composite conductors are insulated because of the native oxides on the LM particles, thus activation process is needed. In this work, mechanical activation was used. As shown in Fig. 4(a) and Fig. S3 in the ESM, the LM particles were insulated by the naturally formed oxides in the initial state, and then external strain was applied to the LM conductor to rupture the native resistive oxidation layer on LM particles and make them coalesce into a percolating network. The resistance changes of the strain activation process are shown in Fig. 4(b). The average thickness of the LM conductors was 24.903 μm. The resistance was drastically reduced to nearly 1 Ω when 20% strain was applied, and further stretching to 100%, resistance decreased to 0.74 Ω. Subsequent cycles of stretching and releasing barely changed the amplitude of resistance changes. The curves of resistance changes of the second to fifth cycle nearly coincided, which demonstrated the successful establishment of a stable and continuous conductive network.

Subsequently, the electronic conductivity of the LM-FR composites was optimized by adjusting the content of the LM. The resistance changes of different content of LM are shown in Fig. 4(c). Four different proportions of LM to FR were tested, and further reducing the content of LM would cause great resistance raising, hence the smallest proportion of LM was chosen as 15:1

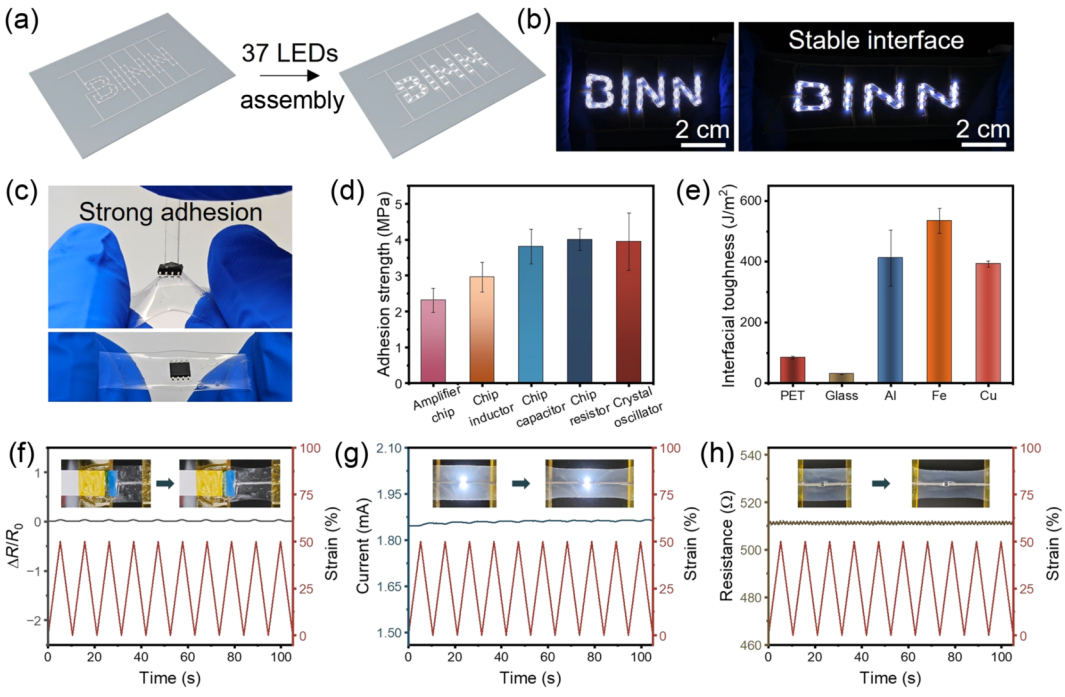

Figure 3 The strong interfacial adhesion of FR substrate for the stretchable hybrid device. (a) Schematic illustration of the fabrication of the circuit line and the LED array assembled for stretchable display. (b) Optical image of the LED array reading "BINN" without strain (left) and with 50% strain (right). (c) Illustration of the strong adhesion between the FR substrate and the chip. (d) The adhesion strength test between the FR substrate and the various electronic components. (e) The interfacial toughness between the FR substrate and the various common materials in electronic circuits. (f)–(h) The electronic response of various hybrid stretchable devices including flexible flat cable, LED, and chip resistor under cyclic strain.

(LM:FR). The resistance changes and the resistance of LM conductor samples after strain activation of different proportions are shown in Fig. 4(c) and the inset of Fig. 4(c), respectively. These results clearly illustrated that the resistance decreased significantly as the content of LM increased, except when the proportion of LM reached 30:1, because the LM particles were extremely unstable under stirring and prone to coalesce into large LM droplets when the proportion of LM reached 30:1. Consequently, this might result in lower real content of LM in the conductor when compared to the proportion of 25:1. Additionally, the LM conductor samples possessed the highest stretchability when the proportion of LM was 25:1, and the conductivity reached 2259.57 S/cm. Because the LM conductor samples all generated cracks under a similar strain, the cracks exerted less impact on the resistance of the LM conductor with the proportion of 25:1 due to the higher electrical conductivity. Moreover, the resistance stability under strain, which was commonly evaluated by the relative resistance change: $\Delta R/R_0 = (R - R_0)/R_0$, was another important parameter for the LM conductor samples. The quantified relative resistance change values of the LM conductors with different proportions under different strains are presented in Fig. 4(d). Obviously, the LM conductors with a proportion of 25:1 emanated the smallest relative resistance changes which were 0.677%, 2.089%, 4.924%, and 8.597% under the strain of 50%, 100%, 200%, and 300%, respectively. Hence, LM conductors with the proportion of 25:1 presented the best electrical properties. Additionally, the strain insensitive behavior of the LM composite conductor might be attributed to the interactions between FR and LM oxides enabled deformation and coalescence of the LM particles [36]. As shown in Fig. S4 in the ESM, a droplet of LM was dropped on the FR film, and then the droplet deformed spontaneously with strain applied on the FR film, which suggested the firm interaction with FR. Hence, the LM particles would deform and coalesce under the hydrostatic pressure transmitted by the FR under external strain. More conductive paths were formed under stretching, thus enabling the strain insensitive behavior. In addition, our LM composite conductor showed comparable comprehensive properties compared with previously reported stretchable conductors (Table S1 in the ESM).

Subsequently, the stability and durability of the LM conductors were studied. The long-term cyclic test was implemented on the LM conductors under 50% strain. As illustrated in Fig. 4(e), after 10,000 cycles of stretching under 50% strain, the LM conductors still maintained very low resistance with their initial resistance only slightly increasing from 1.435 to 1.447 Ω, a small change of only 0.836%. Then we performed more tests on the LM conductors that were more closely aligned with actual application scenarios, including bending, twisting, and pressing. Firstly, the relative resistance change of the LM conductors under bending is shown in Fig. 4(f). It can be clearly observed that the resistance remained almost constant throughout the bending range of 0° to 180°. Next, a twisting test, which was another common type of deformation conductors and would be encountered in actual application, was carried out, and the result is presented in Fig. 4(g). The resistance of the LM conductor slightly increased at the beginning and began to decrease after 3 turns, which might be attributed to the reconstruction of the conductive network. Then, the LM conductor was implemented with a press that combined both stretching and bending, and a high h/l_0 ratio only resulted in a relative resistance change of 1.435. All these above results clearly demonstrate the high conductivity, stability, and durability of the LM conductors, which indicates the great potential in the application of stretchable systems.

3.5 Demonstration of the stretchable hybrid system

To further demonstrate the potential of our strategies in the complex stretchable hybrid systems, we built a stretchable hybrid LED display system and employed it in on-skin visualization of pressure levels. The structure and composition of the stretchable 6 × 6 LED array are shown in Fig. 5(a). Due to the high conductivity and stretchability of the LM conductor and the adhesive FR substrate, it can guarantee reliable contact between

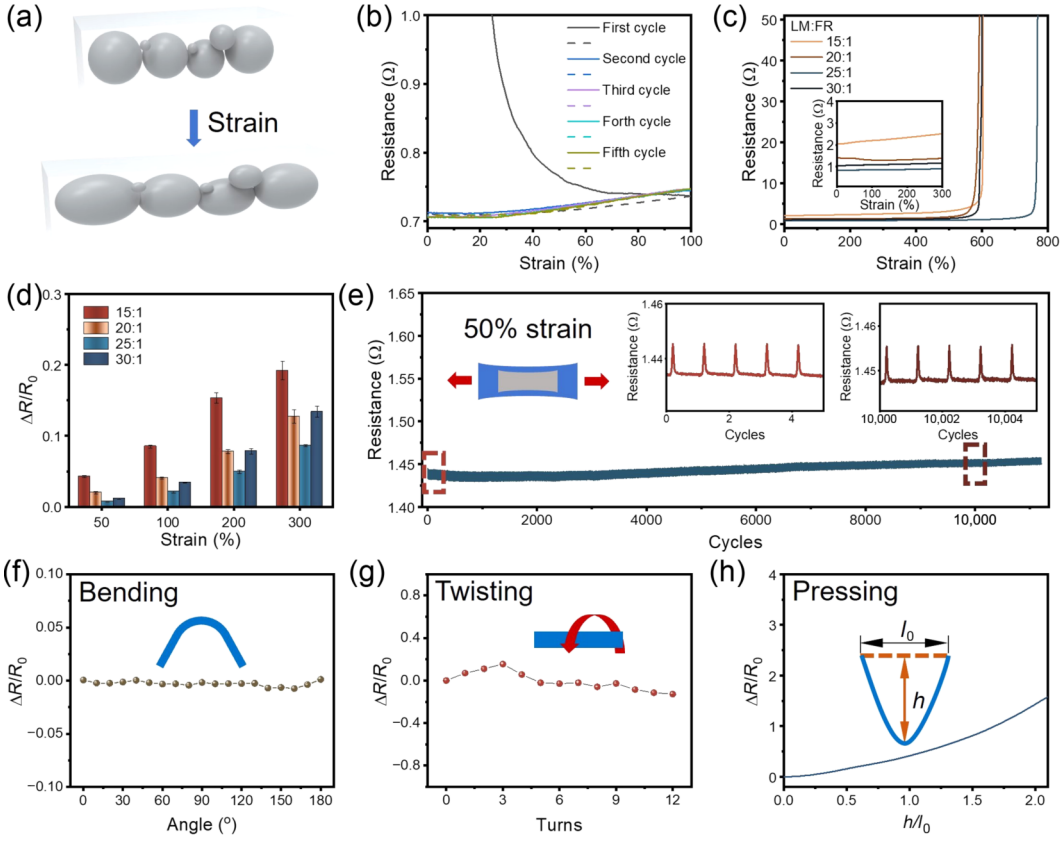

Figure 4 The electronic properties of the strain-insensitive LM conductors. (a) Schematic illustration of the strain activation process of the LM conductors. (b) Resistance changes of the LM conductors under cyclic strain of the activation process. (c) Resistance changes of the LM conductors with different proportions. (d) Quantified relative resistance changes values of different LM conductors with different proportions at fixed strains. (e) Long-term stability test of the LM conductor over 10,000 cycles. (f)–(h) Resistance changes of the LM conductor under bending, twisting, and pressing, respectively.

rigid LED and soft LM conductors and maintain stable connections with the rigid circuit modules through the FPC cables. Therefore, the LED array could effectively satisfy the requirements of displaying the pressure states. The system block diagram of the stretchable hybrid LED display and pressure perception system is illustrated in Fig. 5(b). Specifically, the system comprised three units, including (1) pressure signals acquisition and conversion, (2) microcontroller unit (MCU) for signals processing and instructions transmission, and (3) LED driver enabled LED array to display the corresponding content. The complete procedures of the acquisition, processing, and display are depicted in Fig. 5(c). The pressure signals were firstly captured by the commercial pressure sensor attached to the finger, then the responding signals were converted into voltage signals and transmitted to the MCU. After signals were processed by MCU to discern the pressure state, instructions were sent to the LED driver to enable the LED array to display corresponding content according to the present pressure state, as shown in Fig. 5(d).

The LED array display was mounted on the volunteer's hand (Fig. 5(e)). When grasping with an empty hand (motion A), only the LM conductors connecting the pressure sensor and the conversion module were subjected to external strain, without any pressure being applied to the pressure sensor. Hence there is no discernible response, as shown in Fig. 5(f), and the LED array still displayed "L", indicating the stability of the LM conductor. However, when grasping with increased pressure (motions B to D), the responding signals also increased. The LED array would continue to display "L" when the pressure remained under a safe pressure state. While, if the pressure reaches a state that needs notice, the LED array would change to "H" (for high pressure, indicating a need for notice due to high pressure). Further, when the pressure reaches a critical state, the LED array would coruscate "A" (for attention, indicating a critical pressure state requiring immediate attention) to remind for caution. The above results demonstrated the promising potential applications in complex multifunctional stretchable hybrid systems.

4 Conclusions

In summary, we reported a simple, universal, and scalable strategy for the stretchable hybrid system through a highly precise printable LM composite conductor and adhesive FR substrate. The properties of the LM composites could be easily modulated to satisfy the need for highly precise printing on various substrates, thus realizing a precise line width of 100 μm. On the other hand, the adhesive FR substrate was utilized to overcome the challenge of ensuring the interfacial toughness between rigid and soft modules. The FR substrate could form strong interfacial adhesion between various components and materials through simply pressing and heating, hence ensuring a stable electrical connection. On this basis we prepared several basic stretchable hybrid devices of different components that could stably work under cyclic strain, demonstrating the effectiveness of our strategy. We further successfully fabricated the more complicated 6 × 6 hybrid LED display and pressure perception system that enabled on-skin visualization of pressure levels. With the implementation of our strategy, the simple preparation of complex and multifunctional stretchable hybrid systems that integrate both soft and rigid components is achievable, which might pave the way for the application of on-skin human–machine interaction and soft robotics.

Acknowledgements

The authors thank the support of the National Natural Science Foundation of China (Nos. 52125205, U20A20166, and

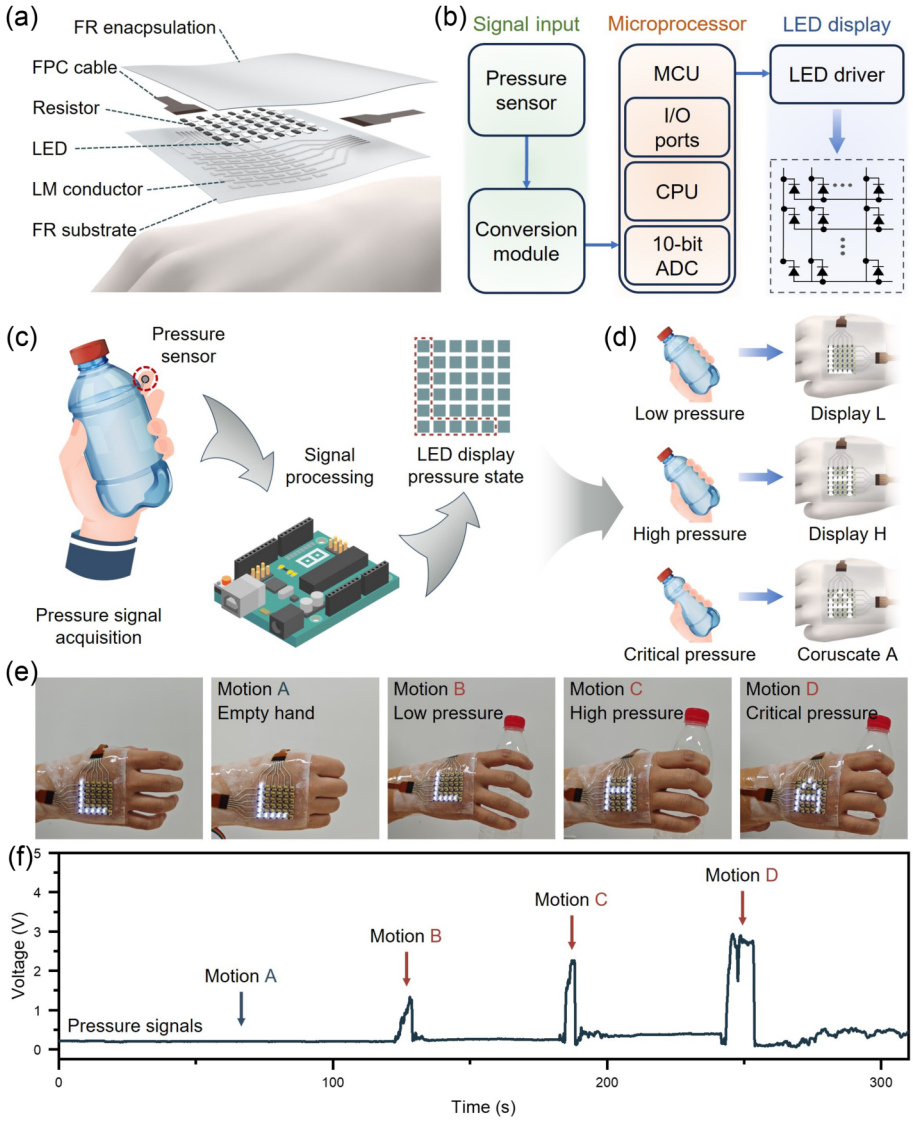

Figure 5 Demonstration of the stretchable hybrid system of pressure perception and display. (a) Schematic illustration of the structure and composition of the stretchable 6 × 6 LED array. (b) The system block diagram of the stretchable hybrid LED display and pressure perception system. (c) and (d) Illustration of the procedures of the signals acquisition, processing, and display. (e) Optical images of the LED array display on hand under different motions. (f) Pressure signals under different motions.

52192614), National Key Research and Development Program of China (Nos. 2021YFB3200302 and 2021YFB3200304), Natural Science Foundation of Beijing Municipality (No. 2222088), Shenzhen Science and Technology Program (No. KQTD20170810105439418), and the Fundamental Research Funds for the Central Universities.

Electronic Supplementary Material: Supplementary material (SEM image, statistical analysis, optical images of the printed circuit, morphology of the LM particles under strain, LM droplet surface reconciliation on FR under strain, table of performance comparison, and supplementary references) is available in the online version of this article at https://doi.org/10.1007/s12274-024-6516-6.

References

[1] Hegde, C.; Su, J. T.; Tan, J. M. R.; He, K.; Chen, X. D.; Magdassi, S. Sensing in soft robotics. *ACS Nano* **2023**, *17*, 15277–15307.

[2] Liu, Y.; Bao, R. R.; Tao, J.; Li, J.; Dong, M.; Pan, C. F. Recent progress in tactile sensors and their applications in intelligent systems. *Sci. Bull.* **2020**, *65*, 70–88.

[3] Bao, R. R.; Tao, J.; Zhao, J.; Dong, M.; Li, J.; Pan, C. F. Integrated intelligent tactile system for a humanoid robot. *Sci. Bull.* **2023**, *68*, 1027–1037.

[4] Zhou, Q. T.; Deng, S. J.; Gao, A. L.; Wang, B. Y.; Lai, J. X.; Pan, J.; Huang, L.; Pan, C. F.; Meng, G. W.; Xia, F. Triboelectric nanogenerator with dynamic electrode for geological disaster and fall-down self-powered alarm system. *Adv. Funct. Mater.* **2023**, *33*, 2306619.

[5] Jiang, Y.; Ji, S. B.; Sun, J.; Huang, J. P.; Li, Y. H.; Zou, G. J.; Salim, T.; Wang, C. X.; Li, W. L.; Jin, H. R. et al. A universal interface for plug-and-play assembly of stretchable devices. *Nature* **2023**, *614*, 456–462.

[6] Zhang, Y. C.; Tan, Y. R.; Lao, J. Z.; Gao, H. J.; Yu, J. Hydrogels for flexible electronics. *ACS Nano* **2023**, *17*, 9681–9693.

[7] Li, J.; Bao, R. R.; Tao, J.; Dong, M.; Zhang, Y. F.; Fu, S.; Peng, D. F.; Pan, C. F. Visually aided tactile enhancement system based on ultrathin highly sensitive crack-based strain sensors. *Appl. Phys. Rev.* **2020**, *7*, 011404.

[8] Wu, W. Q.; Han, X.; Li, J.; Wang, X. D.; Zhang, Y. F.; Huo, Z. H.; Chen, Q. S.; Sun, X. D.; Xu, Z. S.; Tan, Y. W. et al. Ultrathin and conformable lead halide perovskite photodetector arrays for potential application in retina-like vision sensing. *Adv. Mater.* **2021**, *33*, 2006006.

[9] Yu, Y.; Li, J. H.; Solomon, S. A.; Min, J. H.; Tu, J. B.; Guo, W.; Xu, C. H.; Song, Y.; Gao, W. All-printed soft human–machine interface for robotic physicochemical sensing. *Sci. Robot.* **2022**, *7*, eabn0495.

[10] Li, J.; Yuan, Z. Q.; Han, X.; Wang, C. F.; Huo, Z. H.; Lu, Q. C.; Xiong, M. L.; Ma, X. L.; Gao, W. C.; Pan, C. F. Biologically inspired stretchable, multifunctional, and 3D electronic skin by strain visualization and triboelectric pressure sensing. *Small Sci.* **2022**, *2*, 2100083.
[11] Tao, J.; Dong, M.; Li, L.; Wang, C. F.; Li, J.; Liu, Y.; Bao, R. R.; Pan, C. F. Real-time pressure mapping smart insole system based on a controllable vertical pore dielectric layer. *Microsyst. Nanoeng.* **2020**, *6*, 62.
[12] Wang, X. D.; Zhang, Y. F.; Zhang, X. J.; Huo, Z. H.; Li, X. Y.; Que, M. L.; Peng, Z. C.; Wang, H.; Pan, C. F. A highly stretchable transparent self-powered triboelectric tactile sensor with metallized nanofibers for wearable electronics. *Adv. Mater.* **2018**, *30*, 1706738.
[13] Deng, J.; Yuk, H.; Wu, J. J.; Varela, C. E.; Chen, X. Y.; Roche, E. T.; Guo, C. F.; Zhao, X. H. Electrical bioadhesive interface for bioelectronics. *Nat. Mater.* **2021**, *20*, 229–236.
[14] Xue, Y.; Zhang, J.; Chen, X. M.; Zhang, J. J.; Chen, G. D.; Zhang, K.; Lin, J. S.; Guo, C. F.; Liu, J. Trigger-detachable hydrogel adhesives for bioelectronic interfaces. *Adv. Funct. Mater.* **2021**, *31*, 2106446.
[15] Li, G.; Huang, K. X.; Deng, J.; Guo, M. X.; Cai, M. K.; Zhang, Y.; Guo, C. F. Highly conducting and stretchable double-network hydrogel for soft bioelectronics. *Adv. Mater.* **2022**, *34*, 2200261.
[16] Haque, A. B. M. T.; Ho, D. H.; Hwang, D.; Tutika, R.; Lee, C.; Bartlett, M. D. Electrically conductive liquid metal composite adhesives for reversible bonding of soft electronics. *Adv. Funct. Mater*., in press, https://doi.org/10.1002/adfm.202304101.
[17] Song, H. L.; Luo, G. Q.; Ji, Z. Y.; Bo, R. H.; Xue, Z. G.; Yan, D. J.; Zhang, F.; Bai, K.; Liu, J. X.; Cheng, X. et al. Highly-integrated, miniaturized, stretchable electronic systems based on stacked multilayer network materials. *Sci. Adv.* **2022**, *8*, eabm3785.
[18] Hua, Q. L.; Sun, J. L.; Liu, H. T.; Bao, R. R.; Yu, R. M.; Zhai, J. Y.; Pan, C. F.; Wang, Z. L. Skin-inspired highly stretchable and conformable matrix networks for multifunctional sensing. *Nat. Commun.* **2018**, *9*, 244.
[19] Lu, N. S.; Yoon, J.; Suo, Z. G. Delamination of stiff islands patterned on stretchable substrates. *Int. J. Mater. Res.* **2007**, *98*, 717–722.
[20] Zhao, Z. H.; Fu, H. R.; Tang, R. T.; Zhang, B. C.; Chen, Y. M.; Jiang, J. Q. Failure mechanisms in flexible electronics. *Int. J. Smart Nano Mater.* **2023**, *14*, 510–565.
[21] Kim, D. H.; Lu, N. S.; Ma, R.; Kim, Y. S.; Kim, R. H.; Wang, S. D.; Wu, J.; Won, S. M.; Tao, H.; Islam, A. et al. Epidermal electronics. *Science* **2011**, *333*, 838–843.
[22] Xu, S.; Zhang, Y. H.; Cho, J.; Lee, J.; Huang, X.; Jia, L.; Fan, J. A.; Su, Y. W.; Su, J.; Zhang, H. G. et al. Stretchable batteries with self-similar serpentine interconnects and integrated wireless recharging systems. *Nat. Commun.* **2013**, *4*, 1543.
[23] Shyu, T. C.; Damasceno, P. F.; Dodd, P. M.; Lamoureux, A.; Xu, L. Z.; Shlian, M.; Shtein, M.; Glotzer, S. C.; Kotov, N. A. A kirigami approach to engineering elasticity in nanocomposites through patterned defects. *Nat. Mater.* **2015**, *14*, 785–789.
[24] Zhang, Y. F.; Huo, Z. H.; Wang, X. D.; Han, X.; Wu, W. Q.; Wan, B. S.; Wang, H.; Zhai, J. Y.; Tao, J.; Pan, C. F. et al. High precision epidermal radio frequency antenna via nanofiber network for wireless stretchable multifunction electronics. *Nat. Commun.* **2020**, *11*, 5629.
[25] Lacour, S. P.; Chan, D.; Wagner, S.; Li, T.; Suo, Z. G. Mechanisms of reversible stretchability of thin metal films on elastomeric substrates. *Appl. Phys. Lett.* **2006**, *88*, 204103.
[26] Jiang, Z.; Chen, N.; Yi, Z. G.; Zhong, J. W.; Zhang, F. L.; Ji, S. B.; Liao, R.; Wang, Y.; Li, H. C.; Liu, Z. H. et al. A 1.3-micrometre-thick elastic conductor for seamless on-skin and implantable sensors. *Nat. Electron.* **2022**, *5*, 784–793.
[27] Qi, D. P.; Liu, Z. Y.; Liu, Y.; Jiang, Y.; Leow, W. R.; Pal, M.; Pan, S. W.; Yang, H.; Wang, Y.; Zhang, X. Q. et al. Highly stretchable, compliant, polymeric microelectrode arrays for *in vivo* electrophysiological interfacing. *Adv. Mater.* **2017**, *29*, 1702800.
[28] Chen, S.; Hu, K. M.; Yan, S. Z.; Ma, T. J.; Deng, X. L.; Zhang, W. M.; Yin, J.; Jiang, X. S. Dynamic metal patterns of wrinkles based on photosensitive layers. *Sci. Bull.* **2022**, *67*, 2186–2195.
[29] He, J.; Zhou, R. H.; Zhang, Y. F.; Gao, W. C.; Chen, T.; Mai, W. J.; Pan, C. F. Strain-insensitive self-powered tactile sensor arrays based on intrinsically stretchable and patternable ultrathin conformal wrinkled graphene-elastomer composite. *Adv. Funct. Mater.* **2022**, *32*, 2107281.
[30] Jiang, Y. W.; Zhang, Z. T.; Wang, Y. X.; Li, D. L.; Coen, C. T.; Hwaun, E.; Chen, G.; Wu, H. C.; Zhong, D. L.; Niu, S. M. et al. Topological supramolecular network enabled high-conductivity, stretchable organic bioelectronics. *Science* **2022**, *375*, 1411–1417.
[31] Huang, J.; Liu, X. H.; Du, Y. Fabrication of free-standing flexible and highly efficient carbon nanotube film/PEDOT:PSS thermoelectric composites. *J. Materiom.* **2022**, *8*, 1213–1217.
[32] Du, X. J.; Yang, L. Y.; Liu, N. Recent progress on poly(3,4-ethylenedioxythiophene):poly(styrenesulfonate) bioelectrodes. *Small Sci.* **2023**, *3*, 2300008.
[33] Gao, N. W.; Pan, C. F. Intelligent ion gels: Design, performance, and applications. *SmartMat* **2024**, *5*, e1215.
[34] Gao, N. W.; Huang, J. Y.; Chen, Z. W.; Liang, Y. G.; Zhang, L.; Peng, Z. C.; Pan, C. F. Biomimetic ion channel regulation for temperature-pressure decoupled tactile perception. *Small* **2024**, *20*, 2302440.
[35] Ge, G.; Lu, Y.; Qu, X. Y.; Zhao, W.; Ren, Y. F.; Wang, W. J.; Wang, Q.; Huang, W.; Dong, X. C. Muscle-inspired self-healing hydrogels for strain and temperature sensor. *ACS Nano* **2020**, *14*, 218–228.
[36] Zheng, L. J.; Zhu, M. M.; Wu, B. H.; Li, Z. L.; Sun, S. T.; Wu, P. Y. Conductance-stable liquid metal sheath–core microfibers for stretchy smart fabrics and self-powered sensing. *Sci. Adv.* **2021**, *7*, eabg4041.
[37] Hou, X. J.; Zhong, J. X.; Yang, C. J.; Yang, Y.; He, J.; Mu, J. L.; Geng, W. P.; Chou, X. J. A high-performance, single-electrode and stretchable piezo-triboelectric hybrid patch for omnidirectional biomechanical energy harvesting and motion monitoring. *J. Materiom.* **2022**, *8*, 958–966.
[38] Zhu, R. Q.; Li, Z. Y.; Deng, G.; Yu, Y. H.; Shui, J. L.; Yu, R. H.; Pan, C. F.; Liu, X. F. Anisotropic magnetic liquid metal film for wearable wireless electromagnetic sensing and smart electromagnetic interference shielding. *Nano Energy* **2022**, *92*, 106700.
[39] Matsuhisa, N.; Inoue, D.; Zalar, P.; Jin, H.; Matsuba, Y.; Itoh, A.; Yokota, T.; Hashizume, D.; Someya, T. Printable elastic conductors by *in situ* formation of silver nanoparticles from silver flakes. *Nat. Mater.* **2017**, *16*, 834–840.
[40] Jung, D.; Lim, C.; Park, C.; Kim, Y.; Kim, M.; Lee, S.; Lee, H.; Kim, J. H.; Hyeon, T.; Kim, D. H. Adaptive self-organization of nanomaterials enables strain-insensitive resistance of stretchable metallic nanocomposites. *Adv. Mater.* **2022**, *34*, 2200980.
[41] Zhou, K. K.; Zhao, Y.; Sun, X. P.; Yuan, Z. Q.; Zheng, G. Q.; Dai, K.; Mi, L. W.; Pan, C. F.; Liu, C. T.; Shen, C. Y. Ultra-stretchable triboelectric nanogenerator as high-sensitive and self-powered electronic skins for energy harvesting and tactile sensing. *Nano Energy* **2020**, *70*, 104546.
[42] Zhou, K. K.; Xu, W. J. H.; Yu, Y. F.; Zhai, W.; Yuan, Z. Q.; Dai, K.; Zheng, G. Q.; Mi, L. W.; Pan, C. F.; Liu, C. T. et al. Tunable and nacre-mimetic multifunctional electronic skins for highly stretchable contact–noncontact sensing. *Small* **2021**, *17*, 2100542.
[43] Yu, Z. B.; Niu, X. F.; Liu, Z. T.; Pei, Q. B. Intrinsically stretchable polymer light-emitting devices using carbon nanotube-polymer composite electrodes. *Adv. Mater.* **2011**, *23*, 3989–3994.
[44] Xu, H. Y.; Tao, J.; Liu, Y.; Mo, Y. P.; Bao, R. R.; Pan, C. F. Fully fibrous large-area tailorable triboelectric nanogenerator based on solution blow spinning technology for energy harvesting and self-powered sensing. *Small* **2022**, *18*, 2202477.
[45] Lu, Y.; Qu, X. Y.; Zhao, W.; Ren, Y. F.; Si, W. L.; Wang, W. J.; Wang, Q.; Huang, W.; Dong, X. C. Highly stretchable, elastic, and sensitive MXene-based hydrogel for flexible strain and pressure sensors. *Research* **2020**, *2020*, 2038560.
[46] Zhang, H. F.; Xuan, J. Y.; Zhang, Q.; Sun, M. L.; Jia, F. C.; Wang, X. M.; Yin, G. C.; Lu, S. Y. Strategies and challenges for enhancing performance of MXene-based gas sensors: A review. *Rare Met.* **2022**, *41*, 3976–3999.
[47] Han, X.; Qiu, X. Y.; Zong, M.; Hao, J. H. Assembled MXene

macrostructures for multifunctional polymer nanocomposites. *Small Struct.* **2023**, *4*, 2300090.

[48] Ren, J.; Zhang, W. J.; Wang, Y. B.; Wang, Y. X.; Zhou, J.; Dai, L. M.; Xu, M. A graphene rheostat for highly durable and stretchable strain sensor. *InfoMat* **2019**, *1*, 396–406.

[49] Niu, H. S.; Li, N.; Kim, E. S.; Shin, Y. K.; Kim, N. Y.; Shen, G. Z.; Li, Y. Advances in advanced solution-synthesis-based structural materials for tactile sensors and their intelligent applications. *InfoMat* **2024**, *6*, e12500.

[50] Yuk, H.; Zhang, T.; Parada, G. A.; Liu, X. Y.; Zhao, X. H. Skin-inspired hydrogel-elastomer hybrids with robust interfaces and functional microstructures. *Nat. Commun.* **2016**, *7*, 12028.

[51] Hwang, H.; Kong, M.; Kim, K.; Park, D.; Lee, S.; Park, S.; Song, H. J.; Jeong, U. Stretchable anisotropic conductive film (S-ACF) for electrical interfacing in high-resolution stretchable circuits. *Sci. Adv.* **2021**, *7*, eabh0171.

[52] Yuk, H.; Zhang, T.; Lin, S. T.; Parada, G. A.; Zhao, X. H. Tough bonding of hydrogels to diverse non-porous surfaces. *Nat. Mater.* **2016**, *15*, 190–196.

[53] Saiz-Poseu, J.; Mancebo-Aracil, J.; Nador, F.; Busqué, F.; Ruiz-Molina, D. The chemistry behind catechol-based adhesion. *Angew. Chem., Int. Ed.* **2019**, *58*, 696–714.

[54] Cheng, M. J.; Shi, F.; Li, J. S.; Lin, Z. F.; Jiang, C.; Xiao, M.; Zhang, L. Q.; Yang, W. T.; Nishi, T. Macroscopic supramolecular assembly of rigid building blocks through a flexible spacing coating. *Adv. Mater.* **2014**, *26*, 3009–3013.

[55] Li, X.; Deng, Y.; Lai, J. L.; Zhao, G.; Dong, S. Y. Tough, long-term, water-resistant, and underwater adhesion of low-molecular-weight supramolecular adhesives. *J. Am. Chem. Soc.* **2020**, *142*, 5371–5379.

[56] Mredha, M. T. I.; Le, H. H.; Cui, J. X.; Jeon, I. Double-hydrophobic-coating through quenching for hydrogels with strong resistance to both drying and swelling. *Adv. Sci.* **2020**, *7*, 1903145.

[57] Zhang, Y.; Yang, J. L.; Hou, X. Y.; Li, G.; Wang, L.; Bai, N. N.; Cai, M. K.; Zhao, L. Y.; Wang, Y.; Zhang, J. M. et al. Highly stable flexible pressure sensors with a quasi-homogeneous composition and interlinked interfaces. *Nat. Commun.* **2022**, *13*, 1317.

[58] Liu, Z. Y.; Wang, X. T.; Qi, D. P.; Xu, C.; Yu, J. C.; Liu, Y. Q.; Jiang, Y.; Liedberg, B.; Chen, X. D. High-adhesion stretchable electrodes based on nanopile interlocking. *Adv. Mater.* **2017**, *29*, 1603382.

[59] Lee, W.; Kim, H.; Kang, I.; Park, H.; Jung, J.; Lee, H.; Park, H.; Park, J. S.; Yuk, J. M.; Ryu, S. et al. Universal assembly of liquid metal particles in polymers enables elastic printed circuit board. *Science* **2022**, *378*, 637–641.